Emerging beam effects in out-of-plane grating diffraction of He atom beams

Bum Suk Zhao‡, Gerard Meijer and Wieland Schöllkopf

Fritz-Haber-Institut der Max-Planck-Gesellschaft, Faradayweg 4-6, 14195 Berlin, Germany

E-mail: `zhao@fhi-berlin.mpg.de`

Abstract. We report on emerging beam resonances appearing in diffraction patterns of a helium atom beam reflected at grazing incidence from a grating. The plane ruled grating is mounted in an out-of-plane diffraction configuration. We present the measured angular diffraction patterns as a function of the atom's energy change along the grating normal. This presentation allows to readily trace back the peak positions and widths to the geometry of the out-of-plane diffraction configuration. In the diffraction patterns, an interference effect due to emerging beam resonances is found to progress side by side with a new emerging diffraction beam.

PACS numbers: 03.75.Be, 37.25.+k, 42.25.Fx, 68.49.Bc

---

‡ Author to whom any correspondence should be addressed.

1. Introduction

The term *emerging beam resonance*, also known as *threshold resonance*, refers to a general wave diffraction phenomenon that occurs in coherent scattering from a periodic surface. The effect is revealed by abrupt intensity variations of outgoing diffraction beams (including the specular beam) which occur when conditions (i.e. wavelength and incidence angle) are such that another diffracted beam just emerges parallel to the surface. This phenomenon was first observed with visible light by Robert Wood in 1902 [1] and subsequently analyzed by Lord Rayleigh [2]. Therefore, in classical optics, the effect and the conditions for its occurrence are known as Rayleigh-Wood anomaly and Rayleigh conditions (Rayleigh wavelength λ_R and Rayleigh incidence angle θ_R), respectively (see e.g. ref. [3]).

Emerging beam resonances have been predicted by theory to occur for diffraction of atom beams from crystal surfaces [4, 5, 6, 7]. When the incidence angle fulfills the Rayleigh condition, i.e. $\theta_{in} = \theta_R$, the increase of the emerging beam intensity (as a function of incidence angle) is predicted (i) to be of infinite slope and (ii) to perturb the other diffraction beam intensities, $I_n(\theta_{in})$. Here n and θ_{in} denote the diffraction order and the incidence angle, respectively. Thus, the emerging beam resonance is manifested by abrupt intensity variations of outgoing beams, namely, discontinuities of the slope of I_n at the Rayleigh angle of incidence. Emerging beam resonances were expected to occur within an incidence angular range of less than 100 μrad [6]. Under conventional experimental conditions, however, the incident atomic beam divergence is on the order of a few mrad. As a result, the emerging beam effect is smeared out over an incidence angle interval which is more than an order of magnitude wider than the width of the resonance. This experimental constraint was, therefore, identified as one of the main hurdles to experimentally observe emerging beam resonances [6].

Recently, we observed emerging beam resonances in an atom optical experiment, in which a highly collimated helium atom beam is diffracted at grazing incidence from a plane ruled reflection grating of 20 μm period [8]. The high collimation of the incident atom beam and the relatively large grating period allowed us to resolve emerging beam resonances. By varying the incidence angle we observed the resonances precisely at the Rayleigh incidence angles as abrupt variations in the intensities of the diffraction beams and the specular beam.

Here, we report an experimental study of emerging beam effects using a much finer diffraction grating with a period of 0.42 μm. As in the previous experiment, the atom beam impinges upon the grating at grazing incidence. Unlike in the previous experiment, however, the azimuth angle between the plane of incidence and the grating grooves is extremely small. Hence, we observe essentially out-of-plane diffraction. Under these conditions the angular range of the emerging beam resonances increases to more than 500 μrad. As a result, their effect on the diffraction peak intensities is less pronounced. However, in this geometry emerging beam resonances cause anomalous variations of the peak-shapes of the outgoing diffraction beams, which are observed to be correlated with

the progressive emergence of a new diffraction beam.

This paper is organized as follows. The out-of-plane diffraction geometry used in this work is discussed in detail in Section 2, and the experimental apparatus is described in Section 3. The observations are presented and discussed in Section 4, followed by a summary in Section 5.

2. Out-of-plane diffraction geometry

The geometry of the grating and its orientation with respect to the incident atom beam is sketched in Fig. 1(a). The plane of incidence is defined by the incident beam axis and the grating normal. The two essential features of this configuration are: (i) the
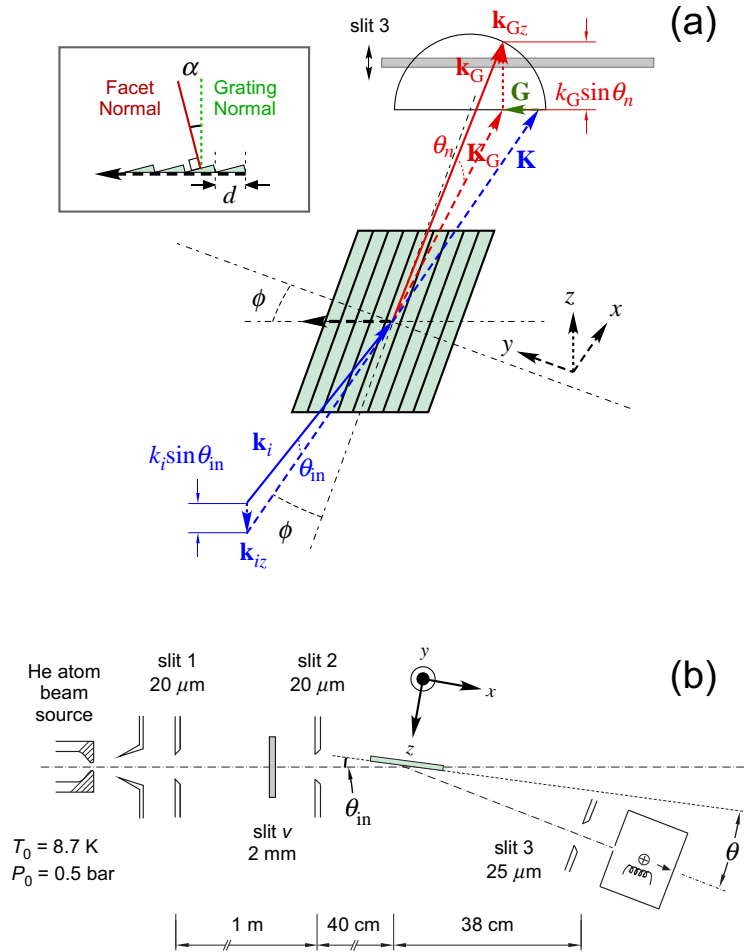

Figure 1. (Color online) (a) Orientation and geometry of the plane ruled diffraction grating. The dashed and dotted lines are parallel and perpendicular to the grating surface, respectively. The grating azimuth angle ϕ (drawn strongly exaggerated) is the angle between the blaze arrow (thick dashed arrow) and the y axis. The detector entrance slit (slit 3) is indicated by the gray bar crossing the semi-circle. For the sake of visibility slit 3, which is parallel to the y axis, is drawn parallel to the blaze angle. (b) Scheme of the experimental setup (top view). In both figures the chosen coordinate system is indicated.

grating is oriented at grazing incidence; and (ii) the grating grooves are close to parallel to the plane of incidence, resulting in out-of-plane diffraction. This mounting geometry has been referred to as *conical diffraction mount* in extreme ultraviolet spectroscopy [9], and it was first applied to grating diffraction of an atom beam in 1996 [10]. The name conical mount relates to the half cone formed by the diffracted wave vectors, as illustrated in Fig. 1(a). Recently, this geometry was employed in scattering of high-energy atomic and molecular beams (kinetic energy $\simeq 1$ keV) from crystal surfaces [11, 12]. In those experiments the semi circle sketched in Fig. 1(a) can be directly visualized by two-dimensional imaging of the fast-atom diffraction spots [13].

The angle of incidence $\theta_{\rm in}$ is defined as the angle between the incident beam axis and the grating surface plane. In the experiments presented here $\theta_{\rm in} \leq 10$ mrad. The grating can be rotated by the azimuth angle ϕ around the z axis, where the plane of incidence and the grating normal are chosen as the xz plane and z axis, respectively. As indicated in Fig. 1, the y axis is perpendicular to the plane of incidence. We define ϕ to be positive when the blaze arrow of the grating is rotated counterclockwise from the y axis as shown in Fig. 1(a). The blaze arrow is illustrated in the inset of Fig. 1(a); it is perpendicular to the grating normal and to the grating grooves, and makes an angle smaller than 90° with the facet normal.

The incident He atom beam is characterized by an incident wave vector $\boldsymbol{k}_i$ ($k_i \equiv |\boldsymbol{k}_i| = 2\pi/\lambda$, λ is the de Broglie wavelength of the atoms) which is indicated in Fig. 1(a) (solid vector). It decomposes into a component $\boldsymbol{K}$ with magnitude $K = k_i \cos\theta_{\rm in}$ parallel to the surface, and a component $\boldsymbol{k}_{iz}$ with magnitude $k_{iz} = k_i \sin\theta_{\rm in}$ perpendicular to the surface. Similarly, the outgoing wave vector is denoted by $\boldsymbol{k}_G = (\boldsymbol{K}_G, \boldsymbol{k}_{Gz})$. For elastic scattering $k_G = k_i$ and, hence, $k_{Gz} = k_i \sin\theta_{\rm n}$, where $\theta_{\rm n}$ is the nth-order diffraction angle, defined with respect to the grating surface. By momentum conservation $\boldsymbol{K}_G = \boldsymbol{K} + \boldsymbol{G}$, which is illustrated in the figure. $\boldsymbol{G}$ is a reciprocal grating vector whose magnitude is given by $G = n2\pi/d$. Here, the diffraction order n is defined positive (negative) when $\theta_{\rm n}$ is larger (smaller) than θ_0. Hence, diffraction beams that are closer to the grating surface than the specular beam are assigned negative orders, whereas positive-order diffraction beams are further away from the surface than the specular beam.

The incoming and outgoing wavevectors are related by energy conservation and satisfy $k_{Gz}^2 = k_i^2 - |\boldsymbol{K} + \boldsymbol{G}|^2$, which can be rearranged as

$$k_{Gz}^2 - k_{iz}^2 = -2KG\cos(\frac{\pi}{2} + \phi) - G^2 \,. \tag{1}$$

Since $k_i = k_G = 2\pi/\lambda$, this equation can be rewritten in the following form

$$\sin^2\theta_{\rm n} - \sin^2\theta_{\rm in} = 2|\sin\phi|\cos\theta_{\rm in}\frac{n\lambda}{d} - \left(\frac{n\lambda}{d}\right)^2 \,, \tag{2}$$

where the artificial introduction of the modulus for $\sin\phi$ is necessary due to our sign convention of n. When $|n\lambda/d| \ll |\sin\phi|$, this equation can be simplified further to $\frac{n\lambda}{(d/|\sin\phi|)} \approx \cos\theta_{\rm in} - \cos\theta_n$, which corresponds to the in-plane grating equation [14] with an effective period $d_{\rm eff} = d/|\sin\phi|$. This simplified in-plane grating equation, which was used successfully in our previous work [8], however, cannot be applied in the

present configuration, since $n\lambda/d = n \times 0.83 \times 10^{-3}$ can not be neglected compared to $\sin\phi = 5 \times 10^{-3}$.

Note that, as a result from Eq. (2), the out-of-plane divergence of the incidence beam, $\delta_\perp$, which could be ignored in previous in-plane helium atom grating diffraction experiments, affects the diffraction patterns in the out-of-plane diffraction geometry. At grazing incidence the out-of-plane divergence causes the azimuth angle to be distributed over an interval of width $\Delta\phi \approx \delta_\perp$ centered at the nominal azimuth angle ϕ. This results in a broadening of the diffraction beams (except for the specular peak with $n = 0$). The finite width of the Rayleigh angle, $\Delta\theta_{R,m}$, for the emergence of the mth-order diffraction beam, is also affected by the out-of-plane divergence of the incident beam, as will be detailed in Section 4.2.

3. Experimental setup

The diffraction apparatus has been described elsewhere before [8, 15, 16]. The continuous helium atom beam is formed by free-jet expansion of ^{4}He gas (99.999% purity) from a source cell (stagnation temperature T_0 and pressure P_0) through a 5-μm-diameter orifice into high vacuum (see Fig. 1(b)). In this work, source conditions are either $T_0 = 8.7$ K and $P_0 = 0.5$ bar or $T_0 = 300$ K and $P_0 = 31$ bar, resulting in a mean velocity (and a corresponding de Broglie wavelength) of the helium atoms of 300 m/s (0.33 nm) or 1760 m/s (0.056 nm), respectively. The relative width of the velocity distribution amounts to less than 1% at $T_0 = 8.7$ K and to about 9% at $T_0 = 300$ K [17].

After passing through a conical skimmer of 500 μm diameter, the beam is collimated by two 20-μm-wide, 5-mm-high vertical slits (slit 1 and slit 2) separated by 100 cm along the beam axis. These slits limit the horizontal (in-plane) beam divergence $\delta_\parallel$ to $\delta_\parallel < 50$ μrad. At a distance of 78 cm downstream from the second slit there is a third vertical slit (slit 3), which is the 25-μm-wide, 5-mm-high detector-entrance slit. The observed angular width (full width at half maximum) of the atom beam is 120 μrad, resulting from a convolution of slit 3 with the divergence-limited beam width. In addition, there is also a 2-mm-high aperture (slit v), located 95 cm downstream from the orifice. This aperture determines the out-of-plane (vertical) divergence $\delta_\perp \approx 2$ mrad.

The detector is a non-commercial mass spectrometer, in which the neutral helium atoms are ionized by electron impact (120 eV electron energy); the ions are accelerated by 1 kV, mass selected by a magnetic 90°-sector field and detected by an electron multiplier tube. The detector, together with slit 3, is mounted on a frame which can be precisely rotated as indicated in Fig. 1(b). The grating is positioned such that the detector pivot axis is parallel to the grating surface and passes through its center. Hence, the pivot axis (vertical) is parallel to the y axis of the reference frame. The detection angle θ is measured with respect to the grating surface plane. Diffraction patterns are obtained by rotating the detector, namely varying θ, and measuring the He signal at each angle. Given the orientation of slit 3 (perpendicular to the plane of incidence) the

high angular resolution of the detector only applies to in-plane scattering.

The grating is a commercial plane ruled grating (Newport 20RG2400-240-1) with 2400 grooves/mm, corresponding to a period $d = 417$ nm, and a blaze angle $\alpha = 16.8°$ (≈ 293 mrad) (see the inset of Fig. 1(a)). It is made out of 6 mm thick glass with an aluminum coating and has a surface area of 5×5 cm^2.

4. Results and discussion

4.1. Diffraction patterns

Diffraction patterns of a helium atom beam at $T_0 = 8.7$ K and $\phi = 5$ mrad are shown in Fig. 2 for various incidence angles. As the right-hand-side of Eq. (2), at grazing incidence, is approximately independent of θ_{in} and θ_n, the observed angular spectra are plotted as a function of $\sin^2 \theta - \sin^2 \theta_{\mathrm{in}}$. Plotted this way, the diffraction peak positions are independent of the incidence angle and, hence, peaks of a given diffraction order appear at the same abscissa position. The abscissa variable, $\sin^2 \theta - \sin^2 \theta_{\mathrm{in}}$, is identical to the kinetic energy change of the He atoms along the grating normal expressed in units of the incident kinetic energy of the atoms.
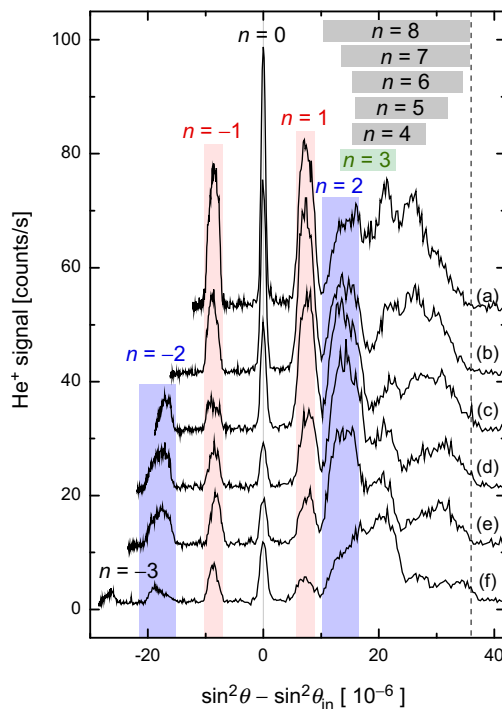

Figure 2. (Color online) Measured angular distributions at $T_0 = 8.7$ K and $\phi = 5.0$ mrad for various incidence angles plotted as a function of $\sin^2 \theta - \sin^2 \theta_{\mathrm{in}}$. The vertical bands indicate the angular spread for $n = -2, -1, 1, 2$ calculated for the azimuth angle range $4 < \phi < 6$ mrad. For $n \geq 3$ the calculated spreads are depicted by bars in the upper right of the graph. The incidence angle θ_{in} is (a) 3.51, (b) 4.01, (c) 4.34, (d) 4.68, (e) 4.84, and (f) 5.34 mrad.

To account for the azimuth angle spread, given by $\Delta\phi \approx \delta_\perp = 2$ mrad centered at $\phi = 5$ mrad, we calculate the diffraction peak positions for the interval $4 < \phi < 6$ mrad. According to Eq. (2), the spread $\Delta\phi$ results in a broadening of the peaks in Fig. 2 by $\Delta\phi\frac{2|n|\lambda}{d}$. Thus, the angular spread $\delta_\perp$ does not affect the specular peak ($n = 0$), but it broadens the other diffraction peaks increasingly with increasing $|n|$. The calculated peak widths are indicated by bars and vertical bands in Fig. 2. In each band the sides close to and far from the specular peak correspond to the calculated peak center for $\phi = 4$ and 6 mrad, respectively.

It is noteworthy that there is a maximum value for $\sin^2\theta - \sin^2\theta_{\rm in}$, above which no helium signal is found in the spectra of Fig. 2. It is inferred from Eq. (2) that $\sin^2\theta_n - \sin^2\theta_{\rm in}$ has a maximum value of $\sin^2\phi\cos^2\theta_{\rm in}$ ($\approx \sin^2\phi$ for grazing incidence), thereby confining the abscissa range of the diffraction spectra. The vertical dashed line in Fig. 2 corresponds to this maximum value for $\phi = 6$ mrad, which agrees well with the
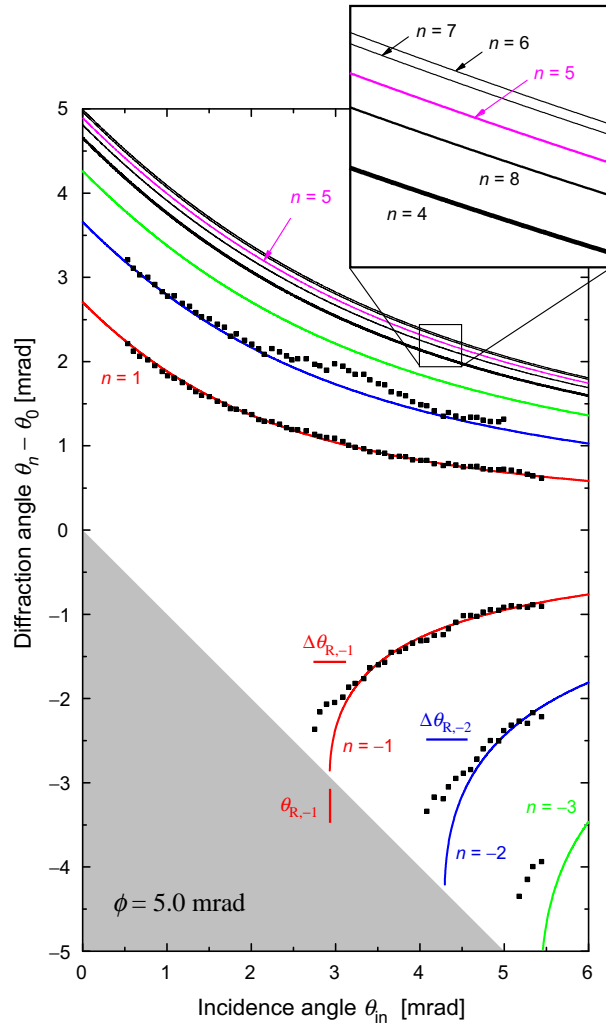

Figure 3. (Color online) Diffraction angle $\theta_n - \theta_0$ as a function of the incidence angle $\theta_{\rm in}$. Experimental measurements are denoted by filled squares for $n = -3$ to 2, while solid curves are theoretical calculations for $n = -3$ to 8 and $\phi = 5.0$ mrad.

experimental observations. The width-indicating bar for $n = 7$ and 8 span up to this maximum. The physics underlying the maximum is the conservation of kinetic energy in the plane perpendicular to the grating grooves, i.e. the plane spanned by the blaze arrow and the z axis. The kinetic energy parallel to the grooves is invariant due to translational symmetry. Eq. (1) can be modified to $k_{Gz}^2 - k_{iz}^2 = K^2 \sin^2 \phi - (K|\sin \phi| - G)^2$, which says that the increase of the kinetic energy along the z axis (left hand side) corresponds to a decrease of the kinetic energy along the direction of the blaze arrow, which is identical to the direction of $\boldsymbol{G}$ (right hand side). Therefore, the maximum increase of the former, proportional to $\sin^2 \theta_n - \sin^2 \theta_{\mathrm{in}}$, is set by the initial value of the latter (i.e. $K^2 \sin^2 \phi$). In the pictorial representation of conical diffraction shown in Fig. 1(a), this maximum corresponds to the apex of the semi-circle.

4.2. Diffraction angles

Fig. 3 shows diffraction angles as a function of the incidence angle θ_{in}. The diffraction angle is defined as the angular separation between the nth and the 0th-order diffraction peaks, $\theta_n - \theta_0$. Squares represent experimental data for $n = -3$ to 2, which have been determined by analyzing a multitude of diffraction patterns (including those plotted in Fig. 2). The peak positions θ_n are determined by fitting a Gaussian to each individual peak of a given diffraction pattern plotted as a function of detection angle θ. The incidence angle θ_{in} is determined from the specular peak position θ_0.

We determine the azimuth angle ϕ by analyzing the data shown in Fig. 3. To this end, Eq. (2) is fitted to the observed 1st-order diffraction angles, with ϕ being the only fitting parameter. The best fit is found for $\phi = 5.0$ mrad. The other solid curves in Fig. 3 are diffraction angles calculated by Eq. (2) for this azimuth angle.

For each diffraction beam of negative order a threshold incidence angle is found below which the beam is diffracted 'into the surface'. This angular region is depicted by the gray shaded area. The threshold angle is the Rayleigh angle $\theta_{\mathrm{R},m}$, indicated by a vertical line in the figure for $m = -1$, where m is the diffraction order of the emerging beam. Furthermore, as shown in the inset, at a given incidence angle the diffraction angles increase until the 6th order, and then start to decrease again from the 7th order on. This reflects the appearance of a maximum diffraction angle in the out-of-plane configuration, as discussed in the previous section.

Discrepancies between theory and experiment are found (i) for the 2nd-diffraction-order in the region around $\theta_{\mathrm{in}} = 3$ mrad and (ii) for the negative orders, which deviate from the theoretical lines near their respective Rayleigh angle $\theta_{\mathrm{R},m}$. The reason for deviation (i) can be seen in Fig. 2, where the angular range of the 3rd order is found to overlap with the one for the 2nd order. This overlap of the peaks causes inaccuracies in the fitting procedure, namely a shift of the fitted peak center towards larger diffraction angles. Deviation (ii) is attributed to the fact that, for incidence angles close to θ_{R}, only a part of the emerging beam has emerged yet, while another part is still below the grating surface [18]. The angular spectrum at $\theta_{\mathrm{in}} = 4.34$ mrad shown in Fig. 2(c)

exemplifies this effect for the -2nd-order peak, which is at the emerging stage with a peak width clearly smaller than the width found once the peak has completely emerged, e.g. at $\theta_{\mathrm{in}} = 4.68$ mrad (Fig. 2(d)). Due to this partial emergence, the fitted peak center position is shifted towards smaller diffraction angles [18].

We define the angular width $\Delta\theta_{\mathrm{R},m}$ as the incidence-angle interval over which the mth-order peak gradually emerges. There are three contributions to $\Delta\theta_{\mathrm{R},m}$: (i) the in-plane divergence $\delta_{\parallel}$; (ii) the out-of-plane divergence $\delta_{\perp}$; and (iii) the de Broglie wavelength spread in the helium atom beam. Considering Eq. (2) these contributions are effective through variations of (i) the incidence angle θ_{in}, (ii) the azimuth angle ϕ, and (iii) the wavelength λ, respectively. For $T_0 = 8.7$ K the relative wavelength spread is just about 1%, and, hence, the effect of (iii) is negligible. The contribution from $\delta_{\parallel}$ is directly seen in the width of the specular peak, shown in Fig. 2, since the right-hand side of Eq. (2) vanishes for $n = 0$. For $n \neq 0$ the dominant contribution to $\Delta\theta_{\mathrm{R},m}$ comes from the out-of-plane divergence $\delta_{\perp}$, discussed above. In Fig. 3 the calculated intervals $\Delta\theta_{\mathrm{R},m}$ are indicated by horizontal lines for the -1st and -2nd diffraction orders. These intervals are seen to coincide well with the regions where discrepancies between the observed and calculated diffraction angles appear.

4.3. Diffraction efficiencies

Diffraction efficiencies, defined as the intensity of the nth-order diffracted beam divided by the incident beam intensity, are plotted in Fig. 4 for three azimuth angles, $\phi = -19$, -6.3, and 5.0 mrad. The beam intensities are determined by analyzing the peak areas in diffraction patterns plotted as a function of detection angle θ. In Fig. 4 Rayleigh angles $\theta_{\mathrm{R},m}$, calculated for each ϕ, are indicated by vertical black solid lines. Around $\theta_{\mathrm{R},m}$ the mth-order peak suddenly emerges and a steep increase of the diffraction efficiency within the incidence-angle interval $\Delta\theta_{\mathrm{R},m}$, also indicated in the figure, is observed.

The diffraction efficiencies of the other beams exhibit minima or at least dips (minima in the first derivative) at or close to the Rayleigh angles. In some cases a kink in the efficiency curve is observed (e.g. in the -1st-order curve for $\phi = -19$ mrad at the -2nd-order emergence). In general these kinks are, however, much less pronounced than those that have been observed previously as a typical fingerprint of emerging beam resonances [8]. We attribute this smoothing-out to the increased $\Delta\theta_{\mathrm{R},m}$ interval, which is about 0.5 mrad in the present experiment as estimated in Figs. 3 and 4. In our previous work it was less than 0.05 mrad due to the small value of $n\lambda/d$ with the same beam geometry $\delta_{\perp}$ [8].

Before the onset of the -1st-order emergence (i.e. to the left of the $\Delta\theta_{\mathrm{R},-1}$ interval) the specular efficiency decreases for all three azimuth angles. During -1st-order emergence the specular efficiency behaves differently for different $|\phi|$. For $\phi = -19$ mrad, the specular efficiency increases, although there are only two data points within $\Delta\theta_{\mathrm{R},-1}$. For $\phi = -6.3$ and 5.0 mrad, on the other hand, the specular efficiency decreases within the range $\Delta\theta_{\mathrm{R},-1}$. This indicates a constructive interference effect on the specular

beam for $\phi = -19$ mrad, but a destructive one for $\phi = -6.3$ and 5.0 mrad. Once the -1st-order beam has fully emerged (to the right of the $\Delta\theta_{R,m}$ interval) the specular efficiency stays about constant for $\phi = -6.3$ and 5.0 mrad, resulting in a kink in the diffraction efficiency curves at the upper end of the $\Delta\theta_{R,-1}$ interval.

In the ideal situation, when $\Delta\theta_{R,m} = 0$ as in plane wave diffraction, only one kink in the diffraction efficiency curve is expected at $\theta_{in} = \theta_{R,m}$, representing the emerging beam resonance. Due to the experimental constraint, however, a new diffraction order emerges within the finite width of incidence angle $\Delta\theta_{R,m}$, thereby smoothing out the emerging beam resonance and make it appear less pronounced.
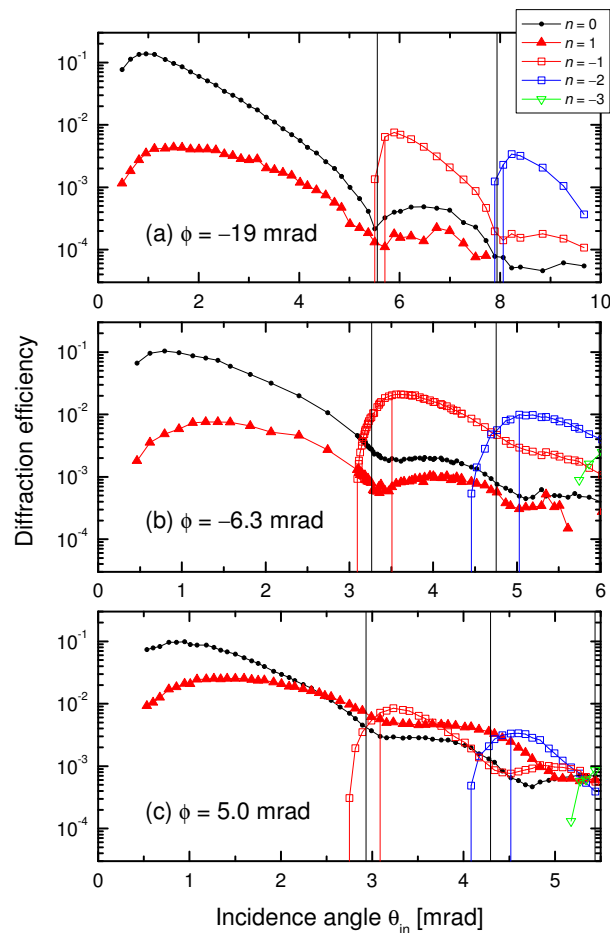

Figure 4. (Color online) Diffraction efficiencies measured at three azimuth angles: (a) $\phi = -19$ mrad; (b) $\phi = -6.3$ mrad; and (c) $\phi = 5.0$ mrad as a function of incidence angles θ_{in} for $T_0 = 8.7$ K. The black vertical lines indicate the position of the Rayleigh angles of incidence where the -1st and -2nd order beams emerge. The boundaries of $\Delta\theta_{R,m}$ are indicated by pairs of colored vertical lines.
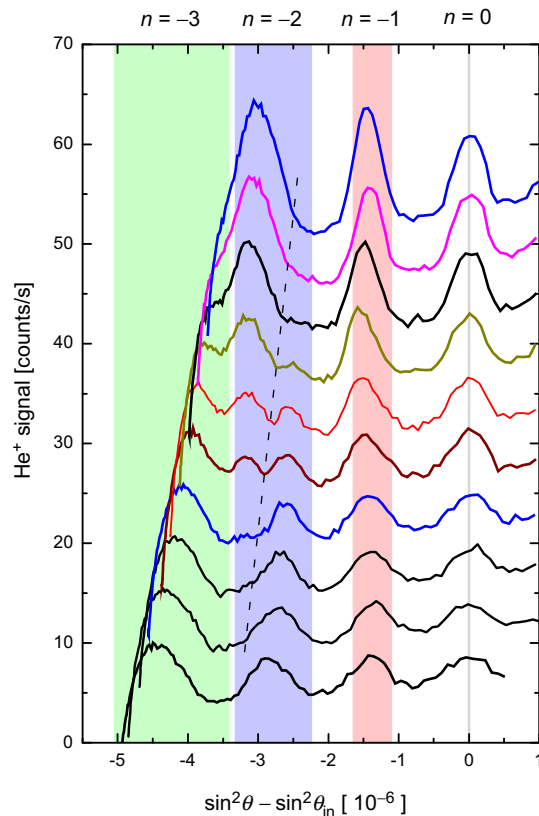
Figure 5. (Color online) Diffraction patterns observed for $T_0 = 300$ K at an azimuth angle $\phi = 5.0$ mrad. The incidence angle is increased from 1.929 mrad (top) to 2.234 mrad (bottom) with an average step size of 0.034 mrad. For diffraction orders $n = -3$, -2, -1, and 0 the vertical bands illustrate the diffraction-angle spread that results for the given azimuth angle spread of $\Delta\phi = 2$ mrad according to Eq. (2). The dashed line indicates a dip marching through the -2nd-order peak while the -3rd-order peak is emerging.

4.4. Emerging beam resonances manifested in peak shapes

Although the kinks in the diffraction efficiency curves are less pronounced than the ones observed previously [8], the present diffraction geometry allows us to observe the effect of emerging beam resonances directly in the angular patterns. Fig. 5 shows a series of diffraction patterns at the emergence of the -3rd-order peak for an azimuth angle of $\phi = 5.0$ mrad. Here, different stagnation conditions, namely $T_0 = 300$ K and $P_0 = 31$ bar, were used. In going from the top to the bottom, the incidence angle is increased from 1.93 to 2.23 mrad. As the -3rd-order peak is emerging from the right to the left within the $n = -3$ band, the -2nd-order peak is first slightly skewed to the left, exhibits a dip moving in the same direction, and is then skewed towards the right. In other words, while the -3rd-order peak is emerging, a clear dip marches through the -2nd-order peak as indicated by the dashed line in Fig. 5. We attribute this dip to a destructive interference within the -2nd-order diffraction beam caused by the emerging beam resonance. This significant variation in peak shape is, therefore,

another manifestation of the emerging beam resonance. It is, in fact, reminiscent of the first observation of the emerging beam resonance effect in 1902 by Robert Wood. Wood observed dark bands (corresponding to the dip found here) in diffraction patterns of light reflected from a ruled grating [1]. In Wood's setup the diffraction beams were wide because he was using a broadband light source, whereas in our setup the widening of the diffraction beams is due to the divergence of the incident beam.

It is remarkable that the diffraction peak shape reflects the resonance already before the onset of emergence of another diffraction beam. This pre-emergence effect can be seen in the diffraction patterns shown in Fig. 6. These angular scans correspond to the data points shown above in Fig. 4(b) ($\phi = -6.3$ mrad) for incidence angles close to the -2nd-order Rayleigh angle. The blue vertical lines in Fig. 4(b) indicate the incidence-angle window of -2nd-order beam emergence between $\theta_{\text{in}} = 4.46$ mrad and 5.03 mrad. The corresponding diffraction patterns are plotted by thick blue lines in Fig. 6. Between these two incidence angles the -2nd-order beam emerges, accompanied by an intensity decrease of the -1st-order peak. Interestingly, already before the first appearance of the -2nd-order peak, i.e., at incidence angles smaller than 4.46 mrad, we find variations in the -1st-order peak shape. For instance, at $\theta_{\text{in}} = 4.09$ mrad (red curve) this peak exhibits a small dip near the top at the right. This dip gets more pronounced when the
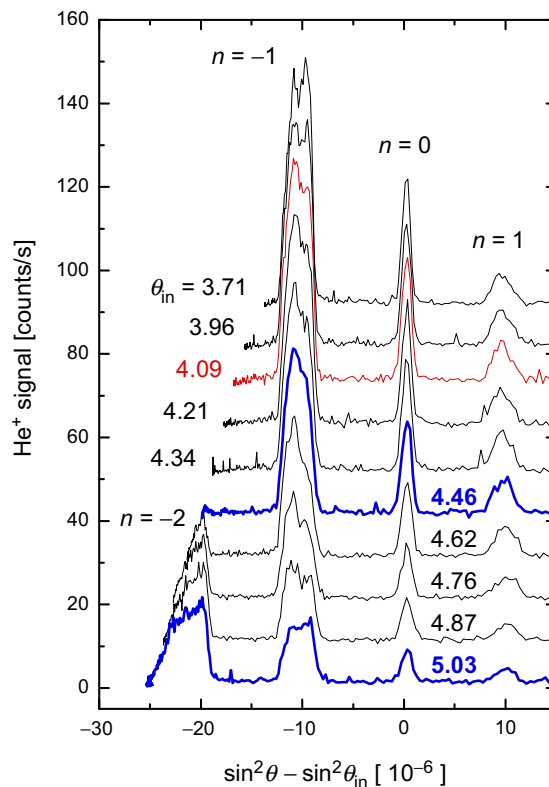

Figure 6. Diffraction patterns observed for $T_0 = 8.7$ K at an azimuth angle $\phi = -6.3$ mrad for various incidence angles. The helium ion signal is plotted as a function of $\sin^2 \theta - \sin^2 \theta_{\text{in}}$, at the Rayleigh condition for $n = -2$.

incidence angle is increased to 4.46 mrad, where the -2nd-order peak starts to appear.

This small dip is possibly caused by the -2nd-order evanescent wave. Before emerging above the grating surface, a diffraction beam is present in the form of an evanescent wave. An evanescent wave is characterized by wave propagation parallel to the surface and an asymptotic exponential amplitude decay along the surface normal direction. Evanescent waves can scatter diffusely from surface defects [19], thereby contributing to a decrease of the coherent surface reflectivity in our experiment. In addition, the evanescent wave (here the -2nd order) can influence the intensities of other outgoing diffraction beams (here the -1st order) through interference. Thus, the dip in the -1st order peak might result from destructive interference with the -2nd order evanescent wave.

5. Summary

In this work diffraction patterns of He atom beams scattering at grazing incidence from a plane ruled blazed grating are presented. The grating is arranged in the conical diffraction mount, i.e., the grating grooves are almost parallel to the plane of specular scattering. The observed diffraction patterns exhibit characteristic features when plotted as a function of the change in the atom's kinetic energy along the surface normal direction. For instance, the diffraction peak width appears to increase substantially with increasing diffraction order, and a maximum possible energy increase along the normal direction is found. These observations are in quantitative agreement with predictions of the conical diffraction model.

The observed diffraction patterns exhibit emerging beam resonances when the incidence angle is close to a Rayleigh angle of incidence, at which another diffraction beam emerges from the grating surface. The emerging beam resonances are manifested as kinks and dips in the diffraction efficiency curve at the Rayleigh angles. Compared to previous measurements with a grating of larger period, however, the kinks are less pronounced. This smearing out of the emerging beam resonances can be attributed to the out-of-plane divergence of the helium atom beam. This divergence causes an effective spread of the grating azimuth angle which, in turn, results in an angular spread of both, the Rayleigh angles and the diffraction angles. Consequently, the diffraction peaks are broadened and the Rayleigh condition is fulfilled for only a part of a diffraction peak. The observation of a dip, marching through a diffraction peak while a new diffraction beam is emerging, represents a clear manifestation of this effect. Peculiarities in the diffraction peak shapes are observed even before the onset of emergence of a new diffraction beam. This pre-emergence effect is attributed to the evanescent wave that describes a diffraction beam before its emergence above the surface. Interference between the evanescent wave and the incident beam can affect the intensity and shape of the outgoing diffraction beams.

Acknowledgments

References

[1] R. W. Wood. On a remarkable case of uneven distribution of light in a diffraction grating spectrum. *Phil. Mag.*, 4(19-24):396–402, 1902.

[2] Lord Rayleigh. Note on the remarkable case of diffraction spectra described by Prof. Wood. *Phil. Mag.*, 14(79-84):60–65, 1907.

[3] R. Petit, editor. *Electromagnetic Theory of Gratings*. Springer, Berlin, 1980.

[4] N. Cabrera and J. Solana. *Proc. Int. School of Physics, Enrico Fermi*, page 530. Compositori, Bologna, 1974.

[5] N. García and W.A. Schlup. Line shapes and threshold resonances for the scattering of waves from surfaces. *Surf. Sci.*, 122(3):L657 – L662, 1982.

[6] G. Armand and J. R. Manson. Threshold resonances in the diffraction of atoms and molecules by surfaces. *Surf. Sci.*, 169(1):216–224, 1986.

[7] R. Guantes, F. Borondo, J. Margalef-Roig, S. Miret-Artés, and J.R. Manson. Threshold resonances in classical chaotic atom–surface scattering. *Surf. Sci.*, 375(2-3):L379 – L384, 1997.

[8] B. S. Zhao, G. Meijer, and W. Schöllkopf. Emerging beam resonances in atom diffraction from a reflection grating. *Phys. Rev. Lett.*, 104(24):240404, 2010.

[9] W. Cash. Echelle spectrographs at grazing incidence. *Appl. Opt.*, 21(4):710, 1982.

[10] R. Brouri, R. Asimov, M. Gorlicki, S. Feron, J. Reinhardt, V. Lorent, and H. Haberland. Thermal atom beam splitting by an evanescent standing wave. *Opt. Commun.*, 124:448–451, 1996.

[11] A. Schüller, S. Wethekam, and H. Winter. Diffraction of fast atomic projectiles during grazing scattering from a LiF(001) surface. *Phys. Rev. Lett.*, 98(1):016103, 2007.

[12] P. Rousseau, H. Khemliche, A. G. Borisov, and P. Roncin. Quantum scattering of fast atoms and molecules on surfaces. *Phys. Rev. Lett.*, 98(1):016104, 2007.

[13] H. Winter, J. Seifert, D. Blauth, M. Busch, A. Schüller, and S. Wethekam. Structure of ultrathin oxide layers on metal surfaces from grazing scattering of fast atoms. *Appl. Surf. Sci.*, 256(2):365–370, 2009.

[14] M. Born and E. Wolf. *Principles of Optics*. Pergamon Press, London, 1959.

[15] B. S. Zhao, S. A. Schulz, S. A. Meek, G. Meijer, and W. Schöllkopf. Quantum reflection of helium atom beams from a microstructured grating. *Phys. Rev. A*, 78(1):010902, 2008.

[16] H. C. Schewe, B. S. Zhao, G. Meijer, and W. Schöllkopf. Focusing a helium atom beam using a quantum-reflection mirror. *New J. Phys.*, 11(11):113030, 2009.

[17] L. W. Bruch, W. Schöllkopf, and J. P. Toennies. The formation of dimers and trimers in free jet ^{4}He cryogenic expansions. *J. Chem. Phys.*, 117:1544, 2002.

[18] J. E. Harvey and E. A. Nevis. Angular grating anomalies: effects of finite beam size on wide-angle diffraction phenomena. *Appl. Opt.*, 31(31):6783–6788, 1992.

[19] D. Farías, M. Patting, K.-H. Rieder, and J. R. Manson. Scattering of He atoms from surface defects by grazing-angle diffraction beams. *Phys. Rev. B*, 65(16):165435, 2002.